Journal of the American Heart Association

ORIGINAL RESEARCH

Age-Associated Changes in Endothelial Transcriptome and Epigenetic Landscapes Correlate With Elevated Risk of Cerebral Microbleeds

Kshitij Mohan, PhD; Gilles Gasparoni, PhD; Abdulrahman Salhab, PhD; Michael M. Orlich, PhD; Robert Geffers, PhD; Steve Hoffmann, PhD; Ralf H. Adams, PhD; Jörn Walter, PhD; Alfred Nordheim, PhD

BACKGROUND: Stroke is a leading global cause of human death and disability, with advanced aging associated with elevated incidences of stroke. Despite high mortality and morbidity of stroke, the mechanisms leading to blood-brain barrier dysfunction and development of stroke with age are poorly understood. In the vasculature of brain, endothelial cells (ECs) constitute the core component of the blood-brain barrier and provide a physical barrier composed of tight junctions, adherens junctions, and basement membrane.

METHODS AND RESULTS: We show, in mice, the incidents of intracerebral bleeding increases with age. After isolating an enriched population of cerebral ECs from murine brains at 2, 6, 12, 18, and 24 months, we studied age-associated changes in gene expression. The study reveals age-dependent dysregulation of 1388 genes, including many involved in the maintenance of the blood-brain barrier and vascular integrity. We also investigated age-dependent changes on the levels of CpG methylation and accessible chromatin in cerebral ECs. Our study reveals correlations between age-dependent changes in chromatin structure and gene expression, whereas the dynamics of DNA methylation changes are different.

CONCLUSIONS: We find significant age-dependent downregulation of the *Aplnr* gene along with age-dependent reduction in chromatin accessibility of promoter region of the *Aplnr* gene in cerebral ECs. *Aplnr* is associated with positive regulation of vasodilation and is implicated in vascular health. Altogether, our data suggest a potential role of the apelinergic axis involving the ligand apelin and its receptor to be critical in maintenance of the blood-brain barrier and vascular integrity.

Key Words: aging ■ blood-brain barrier ■ endothelial cells ■ stroke

Stroke is a leading cause of human death and disability, with 9.6 million cases of ischemic stroke and 4.1 million cases of hemorrhagic strokes occurring globally every year, resulting in 5.5 million deaths.[1] Among surviving patients, a most experience disabilities, with only ≈1 in 4 survivors attaining full functional recovery after 6 months.[2] Advanced aging is a nonmodifiable risk factor associated with stroke, and the incidences of intracerebral hemorrhage in the age groups of 35 to 54, 55 to 74, and 75 to 94 years are reported to be 5.9, 37.2, and 176.3 per 100 000 individuals, respectively.[3] Intracerebral hemorrhage is caused by the rupture of small- to medium-sized blood vessels with a diameter of 100 to 600 μm and is typically a manifestation of cerebral small-vessel disease.[4] Aging is associated with structural, functional, and mechanical changes in small

Correspondence to: Kshitij Mohan, PhD, Division of Cardiovascular Medicine, Radcliffe Department of Medicine, John Radcliffe Hospital, Oxford OX3 9DU, United Kingdom. Email: kshitij.mohan@cardiov.ox.ac.uk

Preprint posted on BioRxiv February 10, 2023. doi: https://doi.org/10.1101/2023.02.10.528012.

This article was sent to Neel S. Singhal, MD, PhD, Associate Editor, for review by expert referees, editorial decision, and final disposition.

Supplemental Material is available at https://www.ahajournals.org/doi/suppl/10.1161/JAHA.123.031044

For Sources of Funding and Disclosures, see page 17.

JAHA is available at: www.ahajournals.org/journal/jaha

RESEARCH PERSPECTIVE

What Is New?

- This is a novel study that comprehensively defines the age-associated changes in gene expression, chromatin accessibility, and genomic methylation levels in the cerebral endothelial cells of aging mice (at 2, 6, 12, 18, and 24 months).
- We identify age-associated downregulation of Apelin (*Apln*) and Apelin receptor (*Aplnr*) gene and reduced chromatin accessibility of the promoter associated with *Aplnr* gene in cerebral endothelial cells, suggesting a potential association of the Apelinergic axis in endothelial dysfunction in aging brains.

What Question Should Be Addressed Next?

- More studies and potential therapeutic targeting of the Apelinergic axis need to be done to conclusively establish the mechanisms by which Apelin regulates blood pressure and vascular integrity.

Nonstandard Abbreviations and Acronyms

ATAC-seq	assay for transposase-accessible chromatin sequencing
BBB	blood-brain barrier
cEC	cerebral endothelial cell
EC	endothelial cell
FACS	fluorescence-activated cell sorting
GFP	green fluorescent protein
MRTF	myocardin-related transcription factor
RNA-seq	RNA sequencing
RRBS	reduced representation bisulfite sequencing
SRF	serum response factor
TGF-β	transforming growth factor-β

blood vessels, resembling the changes in small vessels arising from chronic hypertension. These changes lead to the degeneration of the vascular wall, causing development of small aneurysms and microbleeds in the deeper structures, indicative of risk for intracerebral hemorrhage.[5,6]

The cerebral microvasculature has the unique property of a highly selective blood-brain barrier (BBB) playing an essential role in brain homeostasis by tightly regulating paracellular and transcellular transport of ions, macromolecules, pathogens, and cells of the immune system between blood and brain.[7] The central nervous system's microvasculature comprises a continuous monolayer of endothelial cells (ECs) forming the blood vessels' innermost layer, pericytes that wrap around the ECs, basement membrane surrounding the vascular tube, astrocytes, and neurons.[8] The endothelial monolayer forming the innermost wall of the cerebral microvasculature constitutes the core component of the BBB. The presence of continuous tight junctions that form a physical barrier between the ECs, the adherens junctions, and the basement membrane are the major structures that impart on the cerebral microvasculature its unique characteristic of BBB function.[9,10] Cytoskeletal activities and cell-cell interactions of ECs are regulated to an important extent by the transcription factor serum response factor (SRF).[11–15] Because EC-specific deletion of *Srf* and *Mrtf*, encoding the transcription factors SRF and myocardin-related transcription factor (MRTF)-A/B, respectively, at either postnatal or adult ages, induces lethal cerebral hemorrhages in mice,[15] this study was undertaken with the initial hypothesis that an age-dependent increase in bleeding incidents may be attributable to the age-dependent downregulation of SRF/MRTF function and the dysregulation of SRF/MRTF target genes and other genes responsible for the maintenance of BBB and vascular integrity in cerebral ECs (cECs). However, we did not observe significant age-dependent dysregulation of *Srf* or *Mrtf*.

Increasing age is associated with endothelial dysfunction, as well as functional, structural, and mechanical changes in the blood vessels. Although age is a nonmodifiable risk factor for several vascular diseases, including intracerebral hemorrhage,[6,16] age-dependent changes in expression in cECs are still insufficiently characterized. In this study, we have used RNA sequencing (RNA-seq) to characterize the age-dependent changes in mRNA expression levels in ECs isolated from murine brains at 2, 6, 12, 18, and 24 months.

Furthermore, we interrogated the possibility of age-associated epigenetic regulation of cerebral EC gene expression, primarily focusing on methylation of cytosines in CpG-rich promoter regions of genes.[17] We performed reduced representation bisulfite sequencing (RRBS), a bisulfite conversion-based protocol that enriches CG-rich regions of the genome, to study age-dependent changes in CpG methylation at promoter regions in the cECs isolated from murine brains of increasing age. We also performed an assay for transposase-accessible chromatin sequencing (ATAC-seq) to study the age-associated changes in chromatin landscape of ECs. Our study aims to understand the mechanisms of vascular changes in the brain and in BBB disruption with aging. Our work indicates

epigenetic changes that are partially correlated (ATAC-seq) and noncorrelated (RRBS) with transcriptional changes in ECs of aging brains. We discuss their implications for the risk of aging human individuals encountering stroke.

METHODS

Brief Outline of the Study

We studied the effect of aging on the incidence of spontaneous cerebral bleeding in wild-type mice and studied the underlying age-associated changes in (1) gene expression using RNA-seq, (2) genomic DNA methylation levels using RRBS, and (3) chromatin landscape using ATAC-seq in cerebral ECs.

Data Access and Codes

The raw and processed sequencing RNA-seq, ATAC-seq, and RRBS files have been deposited to Genome Expression Omnibus under the accession number GSE218649. Codes used in the analysis of RNA-seq, ATAC-seq, and RRBS can be provided on request. Other relevant data and protocols used in this study are available from the authors on reasonable request.

Study Approval

The animal experiments performed as part of this project were approved by the Regierungspräsidium Tübingen (Project Nr. Mitteilung nach § 4 Abs, 3 TierSchG, October 18, 2017), and the relevant procedures followed were in accordance with the guidelines of University of Tübingen.

Animal Models

For histologic analysis of bleedings in the brains, C57Bl6 wild-type mice and C57 Bl6 mice having floxed, yet nonrecombined *Srf* and *Mrtf* alleles, were used.[12] These floxed mice do not show any difference in phenotype compared with wild-type mice, and have been used as controls, referred to as control mice henceforth. The mice were generated and housed at the Interfaculty Institute of Cell Biology (Tübingen, Germany). To isolate cECs, the transgenic Cdh5-mT/H2B-GFP mice were used.[18] Two male transgenic Cdh5-mT/H2B-GFP (heterozygous) mice having a C57BL/6J background were provided by Dr Ralf Adams at the Max Planck Institute for Molecular Biomedicine (Münster, Germany). The colony was further expanded at the animal facility in the Department of Molecular Biology at the Interfaculty Institute of Cell Biology (Tübingen, Germany). The mice were kept under a 12-hour day/night cycle (daytime from 6 AM to 6 PM) with ad libitum access to food and water. The mice were randomly checked for the presence of pathogens and infections every 6 months. The mice were maintained according to the regulations pertaining to legal animal protection laws, and the experiments performed as part of this project were approved by the Regierungspräsidium Tübingen (Project Nr. Mitteilung nach § 4 Abs, 3 TierSchG, October 18, 2017). Genotyping of mice was done by polymerase chain reaction (PCR) of ear biopsies. For harvesting brains, the mice were euthanized using increasing concentration of carbon dioxide gas in a gas chamber.

Histopathologic Analysis

Brains were fixed in 4% paraformaldehyde solution at 4 °C for 72 hours, followed by washing under running cold tap water for 3 hours in a beaker. The fixed brain tissues were further treated with increasing concentrations of isopropanol (50%, 75%, 90%, and 100% v/v) followed by Roti-Histol. The processed tissues were then embedded in paraffin and coronally sectioned (Leica rotary microtome RM 2155). Four consecutive sections, each 6 μm, were mounted on an adhesive microscope slide (Marienfeld HistoBond). The sections were dewaxed in Roti-Histol and treated with decreasing concentrations of ethanol (100%, 96%, 80%, and 70% v/v) for rehydration, followed by hematoxylin-eosin staining. The coverslips were mounted with Entellan as the mounting medium.

Microscopic Analysis

Hematoxylin-eosin–stained brain sections were observed under Zeiss Axioplan 2 microscope using an AxioCamHRc camera. To quantify the number of bleedings and microbleedings in each brain, every 10th slide was evaluated, yielding 20 slides per brain for each animal. To quantify, we adhered to the bleedings that had diameter between 50 and 300 μm based on available literature.[19,20] While scoring the microbleeds, the slides were selected in an unbiased manner and blinded to the age of mice from which the brains were harvested. Images of intact and ruptured blood vessels were taken at the same magnification. A blood vessel with extravasation of erythrocytes was counted as bleeding. The number of unique bleedings in a mouse brain was quantified by recording the blood vessels with extravasated erythrocytes that were stained pink in the hematoxylin-eosin staining or by observing the leakage of erythrocytes into the brain parenchyma. We also observed smaller microbleeds and performed a second study focusing on these smaller microbleeds, characterized by smaller size of bleedings (diameter, <30 μm). To quantify the number of small-sized microbleeds in each brain in this study, we evaluated every 10th slide, yielding 20 slides per brain for each animal. The numbers of bleedings and microbleeds across different age groups were statistically analyzed using 1-way ANOVA, followed by the

Tukey honest significant difference test to compare all the possible pairs and test the statistical significance. The analysis was performed using R, and graphs were made using GraphPad Prism version 9.

Purification of ECs

Transgenic Cdh5-mT/H2B-GFP mice were euthanized by exposure to CO_2 gas, followed by cervical dislocation, and their brains were harvested. After washing with ice-cold PBS, each brain was cut into 8 sagittal slices and dissociated using the Adult Brain Dissociation Kit (Miltenyi Biotec), according to the manufacturer's instructions. The cell pellet obtained was resuspended in fluorescence-activated cell sorting (FACS) buffer (1× PBS, 2% FCS, and 2 mmol/L EDTA) to prepare a single-cell suspension from brain. Before sorting, 0.05 μg/mL 4′,6-diamidino-2-phenylindole was added to stain the dead cells, and the single-cell suspension was filtered through a 70-μm cell strainer. The FACS was performed on a BD FACS AriaII (BD Sciences) at the FACS Core Facility Berg, Universitätsklinikum Tübingen. Because the transgenic Cdh5-mT/H2B-GFP mice express, specifically in the ECs, red fluorescence in the cell membrane and green fluorescence in the nuclei, cells double positive for tdTomato and GFP (green fluorescent protein) were sorted using FACS to obtain a pure population of ECs. Single-cell suspensions from brains of littermate wild-type mice lacking the Cdh5-mT H2B-GFP transgene were used as negative controls for FACS. To ensure the highest purity of ECs in the isolated population, we used FACS to sort cells. The GFP^+/$tdTomato^+$ double-positive cells were sorted again for GFP^+/$tdTomato^+$, a process known as reanalysis.

RNA Isolation and RNA-Seq

ECs were directly sorted into RLT Buffer (Qiagen), thereby lysing the cells, and an equal volume of 70% ethanol was added to the lysate. The mRNA was isolated, and DNase digestion was performed using the RNeasy Micro Kit (Qiagen), according to the manufacturer's instructions. Six animals (3 males and 3 females) belonging to the age groups of 2, 6, 12, 18, and 24 months (total n=30) were used for the RNA-seq study. The quality and concentration of the isolated mRNA from each of the 30 samples were assessed using Bioanalyzer RNA 6000 Pico assay (Agilent), with every sample having RNA integrity number >8.3. Full-length cDNA libraries were prepared with the SMART-Seqv4 Ultra Low Input RNA kit (TaKaRa), and the libraries for sequencing were prepared using Nextera XT DNA Library Prep (Illumina), according to the manufacturer's instructions. The libraries were sequenced on Illumina NovaSeq6000 sequencing system at Helmholtz Zentrum für Infektionsforschung (Braunschweig, Germany) and generated 50-bp paired-end reads (PE50).

Assay for Transposase-Accessible Chromatin Sequencing

To study the effect of aging on chromatin accessibility in the cECs, we performed ATAC-seq on ECs isolated from male and female mice belonging to age groups of 2, 6, 12, and 18 months. cECs were sorted into FACS buffer (1× PBS, 2% FCS, and 2 mmol/L EDTA) at 4 °C, and ATAC-seq was performed according to a protocol adapted from Buenrostro et al[21] A total of 50 000 ECs were spun down (500*g*, 5 minutes, 4 °C), supernatant was removed, and the cell pellet was resuspended in cold DNase inhibiting buffer (1 mol/L KCl, 5 mol/L NaCl, 1 mol/L Tris-HCl, 0.5 mol/L EGTA, and 0.5 mol/L spermidine) containing protease inhibitor cocktail (Roche). Then, 0.1% IGEPAL CA-630 (Sigma) was added to the suspension, followed by gently inverting the tube 3 to 4 times and incubation on ice for 5 minutes. The nuclei were spun down (500*g*, 5 minutes, 4 °C), and supernatant was removed and resuspended in the DNase inhibiting buffer. The nuclei were again centrifuged (500*g*, 9 minutes, 4 °C), the supernatant was removed, and the pellet was resuspended in a 50-μL reaction mixture, containing 25 μL 2× TD buffer, 22.5 μL nuclease-free water, and 2.5 μL Tn5 transposase enzyme (Nextera DNA Library Preparation Kit, Illumina, FC-121-1030). The tagmentation reaction was performed at 37 °C for 30 minutes, followed by purification of library using MinElute PCR Purification Kit (Qiagen). The library was eluted in 26 μL elution buffer (Qiagen) and stored at −80 °C until amplification. For amplification, 20 μL library was added to 30 μL PCR mix containing 25 μL NEB Next High Fidelity 2× Master Mix (New England Biolabs), 1 μL each Nextera i5 and i7 indexed primers as forward and reverse primers, and 3 μL nuclease-free water. The amplification was performed in the following steps: 1 cycle of 72 °C for 5 minutes and 98 °C for 30 seconds, 12 cycles of 98 °C for 10 seconds, 63 °C for 30 seconds, and 72 °C for 1 minute, and 1 cycle of 72 °C for 5 minutes. The amplified library was cleaned using 0.8× volume (40 μL) of Ampure beads XP (Beckman Coulter), according to the manufacturer's instruction, and eluted in 20 μL of 0.1× Tris-EDTA buffer. Six animals (3 males and 3 females) belonging to each of the age groups of 2, 6, 12, and 18 months (total n=24) were used for the ATAC-seq study. The quality of the ATAC library was analyzed with Bioanalyzer High-Sensitivity DNA Analysis kit (Agilent), and the concentration of the library was determined using the Qubit HS DNA kit (Life Technologies). The ATAC libraries were sequenced on an Illumina HiSeq2500 sequencing system at the University of Saarland (Saarbrücken, Germany) and

generated ≈50 million 100-bp paired-end reads for each sample.

Reduced Representation Bisulfite Sequencing

A total of 100 000 cECs were sorted in FACS buffer (1× PBS, 2% FCS, and 2 mmol/L EDTA) at 4 °C and centrifuged (500*g*, 5 minutes, 4 °C). The supernatant was discarded, and the cells were snap frozen in liquid nitrogen and stored at −80 °C until further processing. For lysing the cells, 200 μL solution A (25 mmol/L EDTA, 75 mmol/L NaCl), 200 μL solution B (10 mmol/L EDTA, 10 mmol/L Tris-HCl, 1% SDS), and 10 μL Proteinase K (20 μg/μL) were added to the frozen cell pellet, followed by a brief vortex and incubation at 55 °C. Phenol-chloroform-isoamyl (25:24:1) and chloroform-isoamyl (24:1) were used for liquid phase separation of the genomic DNA. Glycogen (20 μg/μL), 0.1× volume (20 μL) of 3M sodium acetate, and 2.5× volume (500 μL) of ice-cold 100% ethanol were added and incubated overnight at −20 °C for precipitation of genomic DNA. The pellet of genomic DNA obtained was washed with 70% ethanol and dissolved in 40 μL prewarmed 1× Tris-EDTA buffer at 45 °C for 2 hours. DNA concentration was measured using a Qubit double-stranded high-sensitivity DNA assay kit (Life Technologies), according to the manufacturer's instructions. Restriction was performed on 26 μL DNA template using 1 μL HaeIII restriction enzyme (New England Biolabs) and 3 μL 10× Cutsmart buffer (New England Biolabs) at 37 °C for 18 hours. A-tailing was performed with 1 μL Klenow fragment (3′→5'exo−, 5 U/μL, NEB) and 1 μL dATP (10 mmol/L, NEB) at 37 °C for 30 minutes, followed by enzyme inactivation at 75 °C for 20 minutes. Unique molecular identifier adapters (TruSeq Single Index Set B, Illumina) were ligated using 1 μL adapters (10 μmol/L), 0.5 μL T4 Ligase (2000 U/μL, NEB), 2 μL ATP (10 mmol/L, NEB), and 1 μL Cutsmart buffer (10×, NEB) at 16 °C for 18 hours, followed by enzyme inactivation at 65 °C for 20 minutes. Bisulfite conversion and subsequent cleanup were performed using EZ-DNA Methylation Gold Kit (Zymo Research), according to the manufacturer's instructions, and the bisulfite-converted genomic library was eluted in 24 μL nuclease-free water. The library was amplified by polymerase chain reaction using 0.6 μL each of primers (10 μmol/L, primer i5: AATGATACGGCGACCACCGAGATCTACAC, primer i7: CAAGCAGAAGACGGCATACGAGAT), 0.6 μL Hot Start Taq (5 U/μL, Qiagen), 3 μL Hotstar PCR Buffer (10×, Qiagen), 1.2 μL $MgCl_2$ (25 mmol/L), and 2 μL dNTPs (10 mmol/L) in a 30-μL reaction with 95 °C for 15 minutes, 20 cycles of 95 °C for 40 s, 58 °C for 1 minute, 72 °C for 1 minute, and 72 °C for 12 minutes, and hold at 4 °C. The amplified RRBS library was cleaned using 0.8× volume (40 μL) of Ampure beads XP (Beckman Coulter), according to the manufacturer's instruction, and eluted in 20 μL of 0.1× Tris-EDTA buffer. Six animals (3 males and 3 females) belonging to each of the age groups of 2, 6, 12, and 18 months (total n=24) were used for RRBS. The RRBS library was analyzed with Bioanalyzer High-Sensitivity DNA Analysis kit (Agilent), and the concentration was determined using the Qubit HS DNA kit (Life Technologies). The sequencing was performed on Illumina HiSeq2500 sequencing system at the University of Saarland (Saarbrücken, Germany) and generated ≈50 million 100-bp single-end reads per sample.

RNA-Seq Data Processing

The preliminary quality control checks on the raw RNA-seq data were performed using FASTQC (v0.11.4) (https://www.bioinformatics.babraham.ac.uk/projects/fastqc/). The 3' adapter sequence (CTGTCTCTTATACACATCTGACGCTGCCGACGA) was trimmed using Cutadapt[22] (v1.15), and quality control checks were again performed on the trimmed reads with FASTQC. The trimmed reads were then aligned to the mouse genome (GRCm38/mm10) using STAR aligner (v2.5.2b).[23] The parameter *quantMode* was set to *GeneCounts* for the calculation of counts per gene. A comprehensive quality report for all the samples was generated with MultiQC[24] (v1.7) (https://multiqc.info/). The counts obtained after STAR alignment were used to study differential expression analysis using DESeq2[25] (v1.24.0). Linear regression analysis was performed on transcripts per million values, calculated by normalizing the raw read counts to the gene length and sequencing depth in each sample, to study the age-associated changes in gene expression. We performed linear regression analysis on RNA-seq data for the 30 samples across all time points (2, 6, 12, 18, and 24 months), adjusting for the sex-specific effects, to identify genes dysregulated in aging. A gene was considered to be significantly dysregulated with age if it had an adjusted $P<0.05$ (*P*.value.age.fdr) in the linear regression analysis (*P*.value.age.fdr refers to the adjusted *P*.value of differentially expressed genes based on age, when corrected after correcting for false discovery rate). We adjusted for multiple testing using the false discovery rate (Benjamini-Hochberg) to discover differentially expressed genes across all time points.

ATAC-Seq Data Processing

The adapter sequence and 3′ ends with base quality (PHRED score) of <20 in the FASTQ files obtained from the sequencing were trimmed with Trim Galore (v0.4.2) software. Following adapter trimming and removing low-quality nucleotides, the FASTQ files were mapped to the mouse reference genome (GRCm38/mm10)

using the GEM[26] mapper. Duplicated reads found after alignment with GEM mapper were annotated with Picard tools (v1.115) (http://broadinstitute.github.io/picard). MACS2[27] (v2.1.0) was used to call nucleosome-depleted regions after down sampling the reads into similar number to avoid any bias in the downstream analyses attributable to sequencing depth. The parameters used in the MACS2 were as follows: –shift –100, –extsize 200, –nomodel, and –keep-dup all. Differentially accessible regions were calculated using a linear model accounting for sex. Peaks that overlap with the black list regions defined by ENCODE (https://doi.org/10.1038/s41598-019-45839-z) were excluded from the analysis.

RRBS Data Processing

Sequencing reads were trimmed using the Trim Galore (v0.4.2) software (http://www.bioinformatics.babraham.ac.uk/projects/trim_galore/) to remove the adapter contamination and the 3′ ends with base quality (PHRED score) of <20. The trimmed reads were then aligned to the mouse reference genome (GRCm38/mm10) using the BWA[28] (v0.6.2) wrapper methylCtools[29] (v0.9.2). Samtools[30] (v1.3) and Picard tools (v1.115) (http://broadinstitute.github.io/picard) were used to convert, merge, and index the alignment files. Single-nucleotide polymorphism aware realignment to identify single-nucleotide polymorphisms for accurate identification of methylated cytosines and methylation calls was performed with the bisulfite single-nucleotide polymorphism calling software Bis-SNP.[31] MethylKit[32] (v1.3.1) was used for tiling (1-kb tiles, minimum 3 CpGs per tile, each CpG with minimum coverage of 5). To identify local age-dependent methylation changes, we applied a 1-kb tiling approach to aggregate single CpG methylation values and used a linear regression model on all obtained 164 020 tiles. Association of DNA methylation and aging was calculated using a linear regression model with sex and coverage as covariates. Obtained *P* values were corrected for multiple testing (false discovery rate) using the Benjamini-Hochberg correction.

RESULTS

Cerebral Bleedings Increase With Age in Mice

Both the wild-type mice and control mice (C57Bl6 mice with floxed, yet nonrecombined, alleles of the *Srf* and *Mrtf* loci) of different ages show an age-dependent increase in spontaneous cerebral bleeding. Notably, the bleedings were of variable sizes (diameter between 50 and 250 μm) and not restricted to any specific brain region (Figure 1B). The average number of bleedings recorded per brain in 2-month-old mice (number of mice used in this age-group, n=4) was 1.75 with an SD of 0.96. In 6- (n=11), 12- (n=11), 15- (n=4), and 25-month-old mice (n=3), the average numbers of bleedings increased to 2.73 (SD, 1.56), 7.72 (SD, 1.35), 13.75 (SD, 0.96), and 17 (SD, 1), respectively (Figure 1E). Although there was no significant increase in the number of bleedings in the brains of the 6-month-old mice compared with the 2-month-old mice (adjusted P=0.73), we noted a significant increase in the bleedings occurring at 12 and 15 months compared with 2-month-old brains (adjusted P<0.001). However, we did not observe a significant increase in the incidents of cerebral bleeding between 15 and 25 months. We further performed Berlin Blue staining on cross-sections of brain chosen randomly to confirm if the bleedings were new and observed that them to be recent (<48 hours old). Because hematoxylin-eosin staining used to quantify bleedings in our study specifically detected fresh cerebral bleedings,[33] and we further performed a confirmatory Berlin Blue staining where we observed all but 1 sample testing negative for the presence of hemosiderin, we argue that the increase in the number of bleedings observed with advancing age in mice is not merely accumulation of old bleedings over time but rather indicates an increase of the incidents of new bleedings with advancing age (Figure S1 and Table S1).

Small-Sized Cerebral Microbleeds Increase With Age in Mice

The wild-type and control mice of different ages also revealed an increased frequency of smaller microbleeds (Figure 1D) with aging. The average number of microbleeds recorded per brain, quantified in serial sections using every 10th slide, in the 2-month-old mice (number of mice used in this age-group, n=4) was 4.5 with an SD of 1.29. At the ages of 6 (n=8), 12 (n=8), and 15 months (n=4), the average numbers of bleeding recorded were 8.75 (SD, 2.39), 13 (SD, 2.62), and 18.5 (SD, 3.11), respectively (Figure 1F). Although there was no significant increase in the number of bleedings in the brains of mice at 6 months compared with 2 months (adjusted P=0.29), we found a significant increase in the bleedings that occur in 12- and 15-month-old mice compared with the 2-month-old mice (adjusted P<0.001). Because brain sections from 25-month-old samples were not available for analysis of the smaller cerebral microbleeds, we only quantified the number of smaller microbleeds in the 2-, 6-, 12-, and 15-month-old age groups. Also, we did not quantify the number of microbleeds in 3 samples belonging to the 12- and 15-months-old groups, accounting for the difference in the total number of brains examined for bleedings and smaller microbleeds.

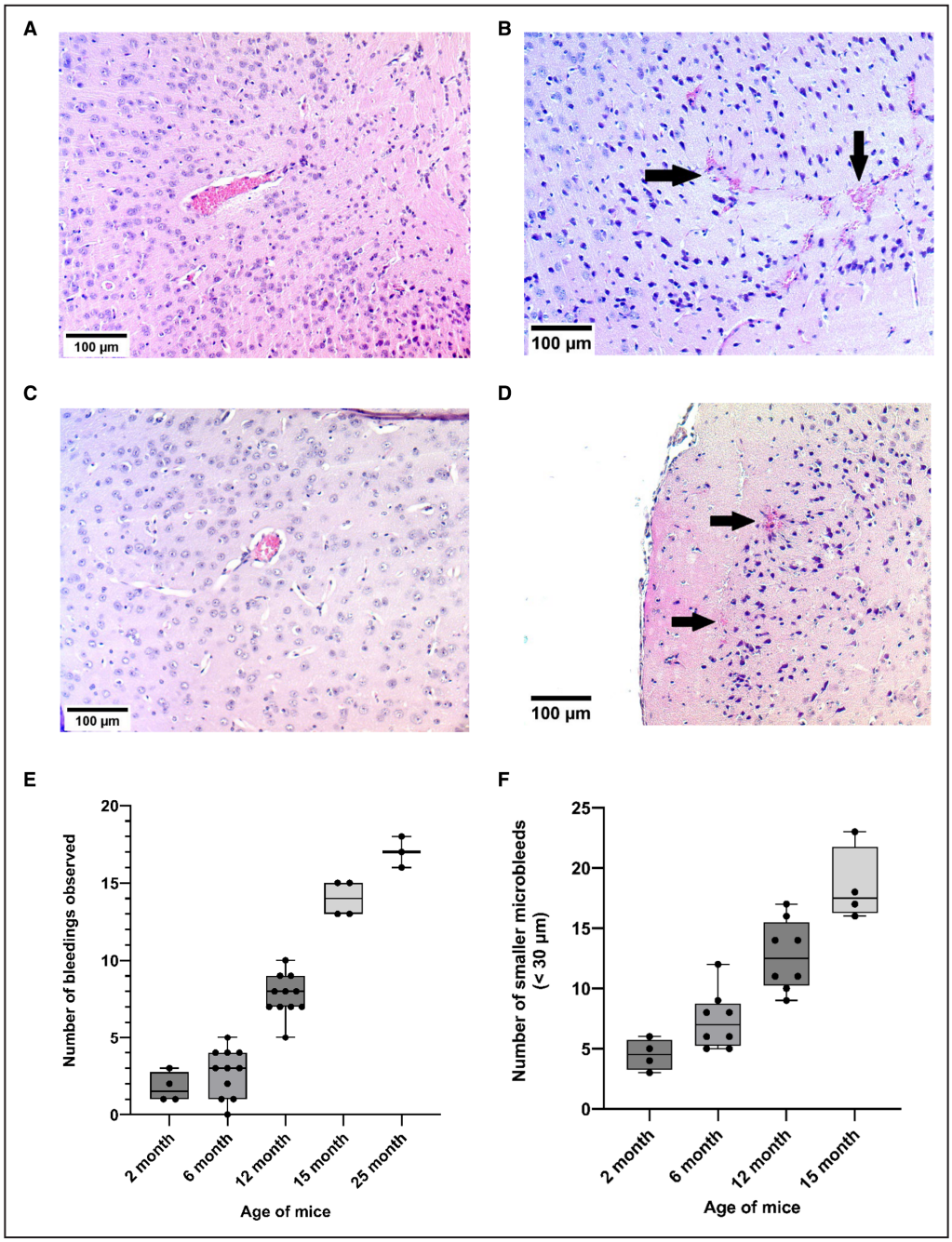

Figure 1. The number of bleedings in the brain of mice increases with age.
A, An intact blood vessel. **B**, Cerebral bleedings from a blood vessel and the leakage of erythrocytes (arrows) stained pink by hematoxylin-eosin (H&E) in the brain parenchyma. **C**, An intact smaller blood vessel in the mouse brain. **D**, Smaller microbleeds from a blood vessel and the leakage of erythrocytes (arrows) stained pink by H&E in the brain parenchyma. **E**, Quantification of bleedings indicates an age-dependent increase in the number of bleedings in the brain. The average number of bleedings recorded per brain in 2-month-old mice (number of mice, n=4) is 1.75. In 6- (n=11), 12- (n=11), 15- (n=4), and 25-month-old mice (n=3), the average numbers of bleedings recorded were 2.73, 7.72, 13.75, and 17, respectively. Error bars represent mean±SEM. **F**, Quantification indicates an age-dependent increase in the number of microbleeds in the brain. The average number of microbleeds recorded (every 10th slide was quantified) per brain in 2-month-old mice (number of mice, n=4) is 4.5. In 6- (n=8), 12- (n=8), and 15-month-old mice (n=4), the average numbers of microbleeds (every 10th slide was quantified) were 8.75, 13, and 18.5, respectively. Error bars represent mean±SEM.

Purification of cECs From Cdh5-mT/H2B-GFP Mice

To purify ECs from the brain vasculature, we took advantage of transgenic *Cdh5-mT/H2B-GFP* mice (Figure 2). We also measured the body weight and weights of different organs but did not observe any age-associated changes (Figure S2 and Table S2). When we analyzed single-cell suspensions prepared from transgenic animals using FACS, ≈7% of the cells were positive for both GFP and tdTomato. A double-positive GFP$^+$/tdTomato$^+$ cell population was absent in the single-cell suspension prepared from wild-type, nontransgenic mouse brains. On the basis of reanalysis,

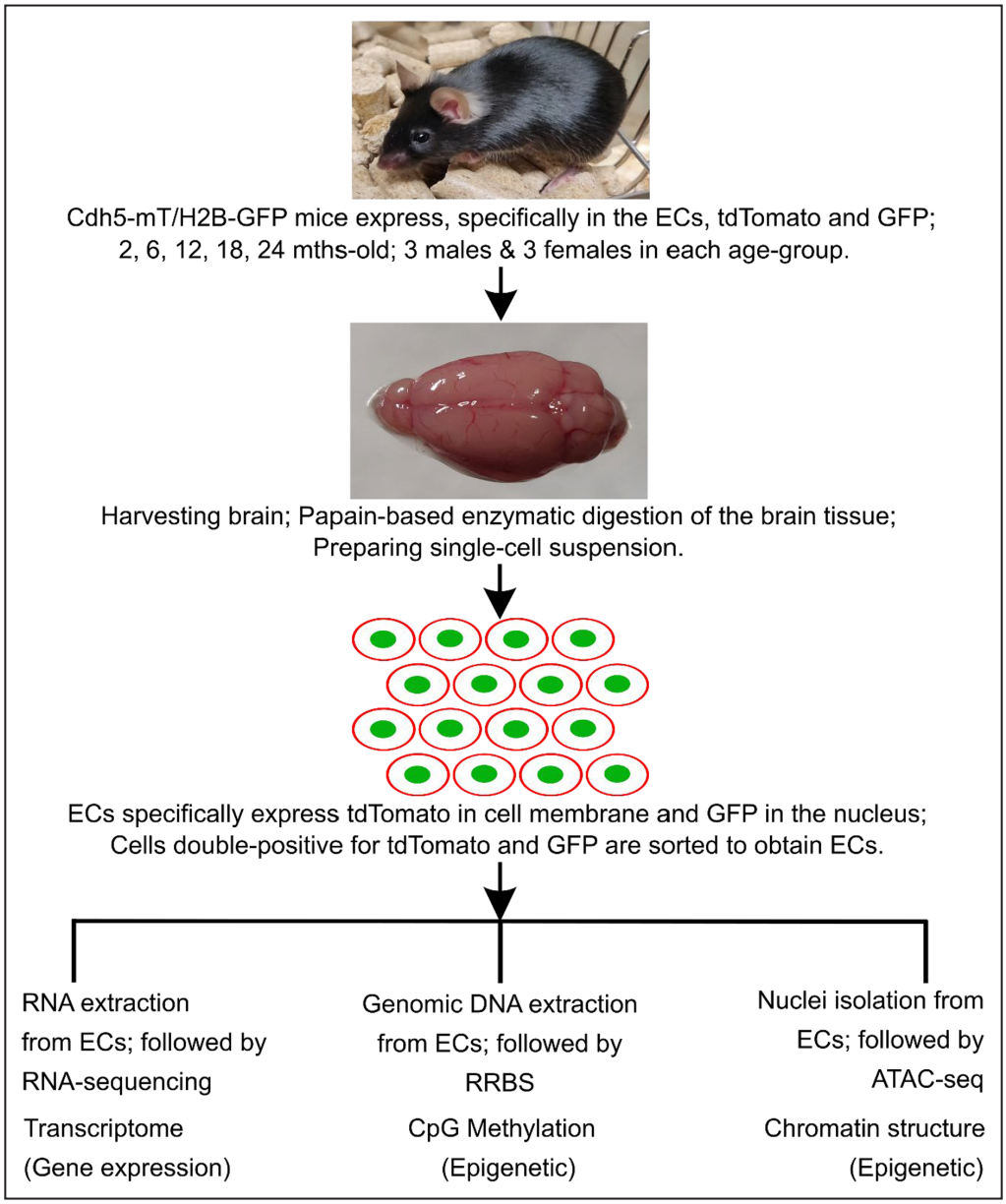

Figure 2. Experimental design to study age-associated transcriptomic and epigenetic changes in the cerebral endothelial cells (cECs).
Cdh5-mT/H2B-GFP transgenic mice that specifically express membrane-targeted tandem dimer Tomato fluorescence and H2B-GFP in endothelial cells (ECs), thereby expressing Tomato fluorescence in the cell membrane and GFP (green fluorescent protein) in the nucleus, were used to isolate pure population of cerebral ECs. A total of 3 male and 3 female mice from each of the 2-, 6-, 12-, 18-, and 24-month-old cohorts were used for the study. RNA sequencing, reduced representation bisulfite sequencing (RRBS), and assay for transposase accessible chromatin sequencing (ATAC-seq) were performed to study age-associated transcriptomic and epigenetic changes (CpG methylation and chromatin accessibility) in the cECs.

we determined the yield of ECs in the sorted cells to be ≈99%. (Figure 3A and 3C and Figure S3). The purity of the isolated EC population was further confirmed using data obtained from RNA-seq of sorted GFP⁺/tdTomato⁺ cells by comparing the relative transcript levels of specific markers for ECs (*Slco1a4*, *Slc1a2*, *Cldn5*, *Flt1*, and *Vwa1*), pericytes (*Pdgfrb*, *Mcam*, *Abcc9*, *Kcnj8*, and *Cspg4*), astrocytes (*Slc1a2*, *Aqp4*, *Gfap*, *S100b*, and *Aldh1l1*), microglia (*Tmem119*, *Cx3cr1*, *Aif1*, *Ptprc*, and *Itgam*), oligodendrocytes (*Olig1*, *Mog*, *Olig2*, *Cldn11*, and *Olig3*), neurons (*Eno2*, *Syp*, *Syt1*, *Rbfox3*, and *Dlg4*), and Schwann cells (*Mobp*, *Mag*, *Gap43*, and *Mpz*). To choose specific markers for different cell types in brain, we used the molecular atlas of cell types in the brain vasculature.[34] As expected, transcripts of EC-specific markers were highly expressed (normalized counts, >100 000) in sorted cells. In contrast, the expression of transcripts of markers of other cells of the neurovascular unit and neural cells were low (normalized counts, ≈1000) to absent, confirming the high level of purity of our EC population (Figure 3D).

RNA-Seq Reveals Age-Dependent Dysregulation of Gene Expression in cECs

In RNA-seq data of cECs, we observed a total number of 30 812 expressed genes, of which 1388 were

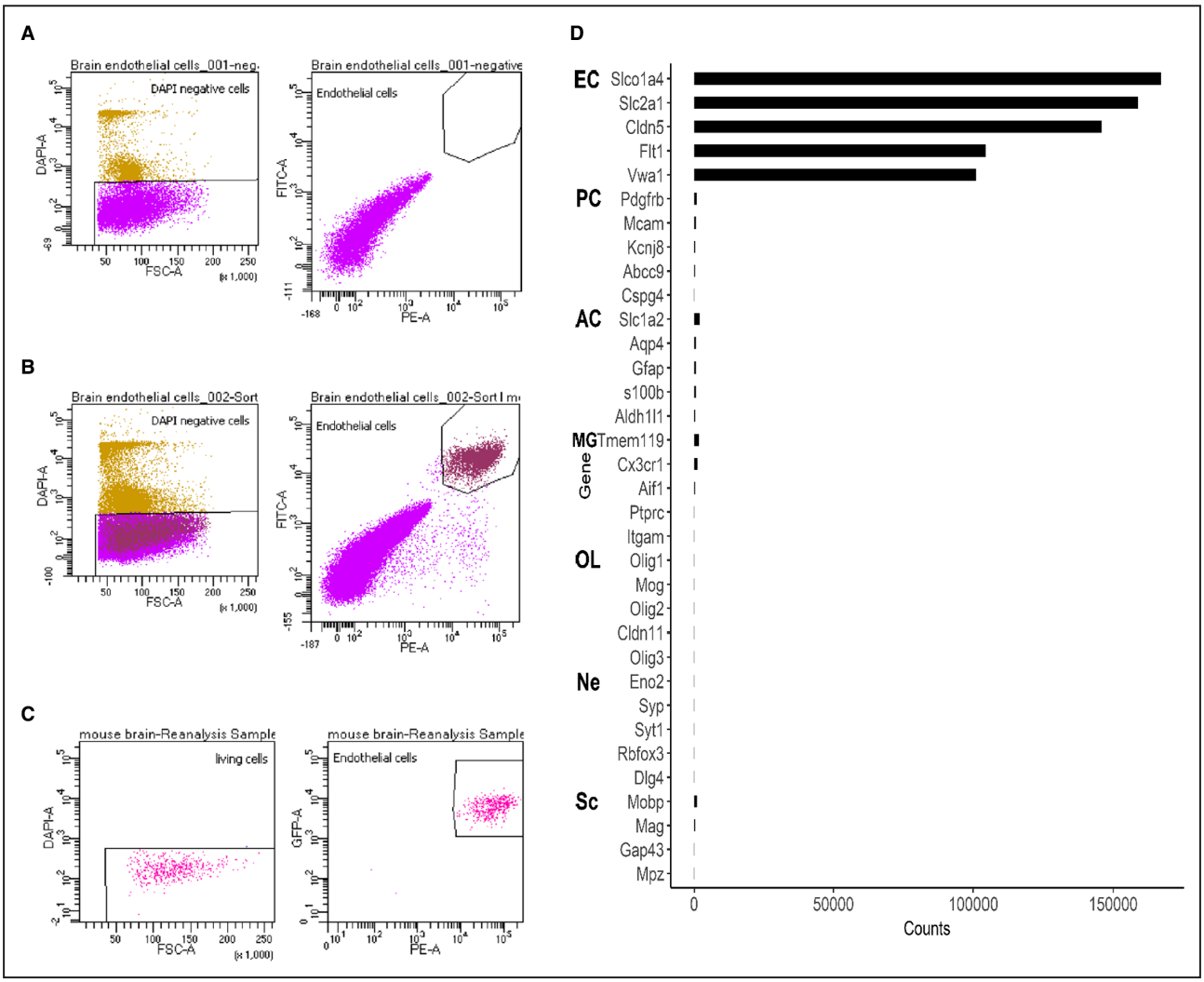

Figure 3. Fluorescence-activated cell sorting profile of sorted endothelial cells (ECs).
A, The single-cell suspension prepared from a wild-type mouse brain does not show a population of cells positive for GFP (green fluorescent protein) and tdTomato. **B**, The single-cell suspension prepared from a Cdh5-mT H2B-GFP transgenic mouse brain shows the presence of EC population double positive for GFP and tdTomato fluorescence. **C**, The double-positive cells (GFP⁺ tdTomato⁺) were sorted. The purity of sorted ECs was ≈99%, as confirmed by the reanalysis of the sorted cells. **D**, The relative transcript levels of specific markers for various cells of the neurovascular unit and the brain. The specific markers for ECs were highly enriched in comparison to the markers for other cells of the neurovascular unit, confirming the purity of the ECs sorted. AC indicates astrocytes; DAPI, 4′,6-diamidino-2-phenylindole; FITC, fluorescein isothiocyanate; MG, microglia; Ne, neurons; OL, oligodendrocytes; PC, pericytes; and Sc, Schwann cells.

significantly dysregulated with increasing age. A total of 675 of these genes were downregulated, whereas 713 were upregulated, with increasing age (Table S3). The significantly dysregulated genes reveal distinctive, age group–specific expression patterns (Figure 4A and Figures S4 and S5). Enrichment analysis performed on the top 1000 genes dysregulated with age in the cECs reveal 345 Gene Ontology (GO) processes that are enriched (Table S4). The processes cardiovascular system development (GO: 0072358), vasculature development (GO: 0001944), regulation of blood vessel endothelial cell migration (GO: 0043535), blood vessel morphogenesis (GO: 0048514), and regulation of endothelial cell migration (GO: 0010594), associated with cerebral vasculature, were among the most enriched processes. We also found enrichment of processes associated with actin dynamics, cytoskeleton organization, and Cdc42 signaling pathway (Tables S5 and S6 and Figures S6 and S7).

We also performed candidate searches and specifically examined the expression patterns of (1) genes implicated in hypertension and associated with human cerebral small-vessel diseases, (2) genes encoding structural components associated with the ECs in BBB, and (3) genes involved in the maintenance of vascular integrity in the brain. We identified both the *Aplnr* gene, encoding Apelin receptor, and the gene encoding its ligand Apelin (*Apln*) to be strongly downregulated with age. We observed that both *Aplnr* and *Apln* display a significant, progressive decrease in expression with age in cECs, as indicated by pair-wise comparison of different age groups. The $\log_2$ fold change values of *Aplnr* were −3.18, −4.10, −4.51, and −5.24 (adjusted $P<0.001$) in 6-, 12-, 18-, and 24-month-old male mice, respectively, compared with 2-month-old mice. In females, the $\log_2$ fold change values of *Aplnr* of 6-, 12-, 18-, and 24-months-old mice were −3.30, −3.47, −4.54, and −4.98 (adjusted $P<0.001$), respectively. Thus, *Aplnr* transcript levels in the cerebral ECs continue to steadily decline during aging from an ≈10-fold change (2 versus 6) to an ≈32-fold change (2 versus 24) even after 6 months of age (Figure 4B). The Apelin signaling pathway is downstream of Notch signaling, with Notch signaling negatively regulating Apln.[35] In zebrafish and human umbilical vein ECs, inhibition of Notch resulted in the upregulation of Apln, whereas activation of Notch led to the inhibition of Apln.[35] We then focused on the Apelin signaling pathway (Kyoto Encyclopedia of Genes and Genomes: mmu04371) and compared the expression of relevant pathway genes with our RNA-seq data. Interestingly, we observed that *Notch3* was significantly upregulated with age.

Next, we attempted to identify age-dependent changes in transcripts of genes encoding structural components in the BBB endothelium. Among the tight junction components, we found a downregulation of the *Cldn5* gene, the major claudin expressed in the ECs of the central nervous system. The linear regression analysis suggests age-dependent downregulation of the *Cldn5* gene (adjusted $P=0.009$) with a correlation coefficient (r^2 value) of 0.42, meaning that 42% of the changes in the expression level of *Cldn5* gene can be correlated with aging. We observed no age-dependent dysregulation of other claudin isoforms, such as *Cldn1*, *Cldn2*, *Cldn3*, *Cldn10*, *Cldn11*, and *Cldn12*, or *Ocln* (occludin), another key component of the tight junctions at BBB. Among junctional adhesion molecules, we found the *F11r* gene encoding the JAM-A protein to be significantly downregulated, whereas *Jam2*, *Jam3*, and *Igsf5* were not significantly dysregulated (Figure 4C).

The age-dependent changes concerned a set of interesting genes associated with the enriched GO terms. *Cdh2* gene (N-cadherin) was downregulated in cECs, whereas no age-dependent dysregulation of *Cdh5* (VE-cadherin) was observed. The same holds for *Cdh1*, β-catenin (*Ctnnb1*), α-catenin (*Ctnna1*), p120 (*Ctnnd1*), and plakoglobin (*Jup*) (Figure S8). Among genes linked to cytoskeleton organization, a significant age-associated downregulation of *Cdc42* (adjusted $P=0.005$) and *Cdc42se1* (adjusted $P=0.003$) was seen as well as changes in the expression of *Arf1* and *Arf6* genes involved in maintaining the actin cytoskeleton dynamics by acting downstream to Cdc42 in the actin polymerization pathway. However, no age-dependent dysregulation was observed in *RhoA*, *Rac1*, *Vcl*, *Vasp*, *Anln*, and *Actn4*, encoding various other actin-binding proteins or tight junction complexes (Figure S9), major scaffolding proteins (Figure S10), extracellular matrix components, such as *Col4a1* and *Col4a2*, laminins, such as *Lama2*, *Lama5*, *Lamb1*, and *Lamc1*, or isoforms of integrins αvβ3, α5β1, α6β1, α1β1, α6β4, and αv (Figure S11).

In human patients, a loss-of-function mutation in the *HTRA1* gene leads to the development of cerebral autosomal recessive arteriopathy with subcortical infarcts and leukoencephalopathy, a rare cerebral small-vessel disease, in which patients display stroke-like symptoms. The *HTRA1* gene encodes a serine protease that regulates TGF-β (transforming growth factor-β) signaling necessary to maintain vascular integrity in the brain. We observed a significant age-dependent downregulation of *Htra1* in cerebral murine ECs, as revealed by the linear regression analysis of our RNA-seq data. Pairwise comparison suggests a significant downregulation of the *Htra1* gene in the 18- and 24-month-old males compared with the 2-month-old group. The $\log_2$ fold change of *Htra1* in 18-month-old mice was −1.5 (adjusted $P<0.001$), and it was −1.31 in 24-month-old mice (adjusted $P<0.001$), indicating ≈3-fold downregulation in the expression of *Htra1* in the cECs of old mice. We also observed a significant age-dependent downregulation of the *Mfsd2a* gene, encoding major

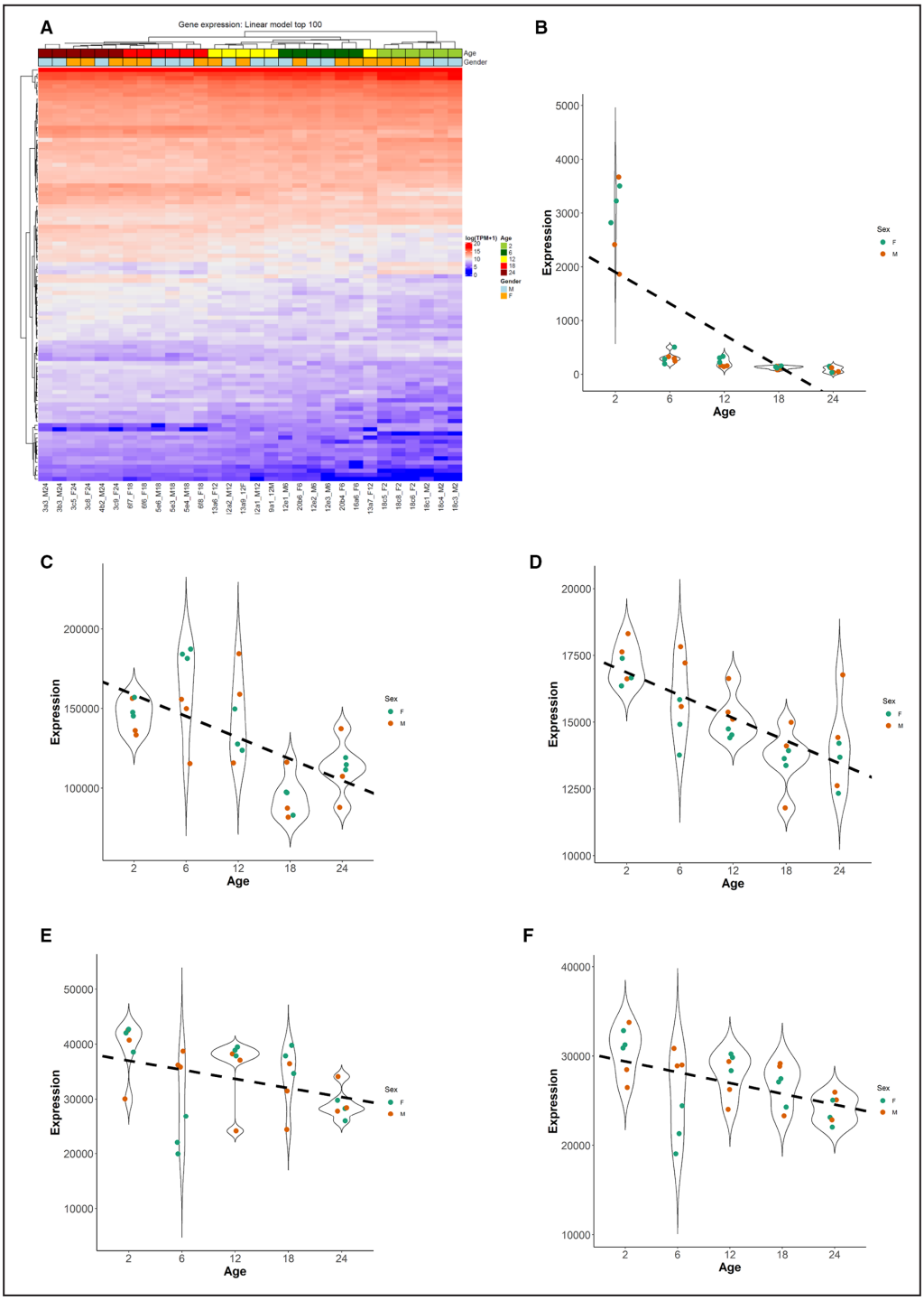

Figure 4. RNA sequencing of cerebral endothelial cells suggests an age-associated dysregulation of genes.

A, Heat map clustering of the top 100 genes exhibits an age-dependent dysregulation based on the linear regression model. **B**, Linear regression analysis suggests that the expression of *Aplnr* decreases with age, with a correlation coefficient (r^2 value) of 0.47 (adjusted P=0.004). The plot showing the normalized counts of *Aplnr* in each sample indicates the downregulation of *Aplnr* is the sharpest between the ages of 2 and 6 months. The violin plots with linear regression analysis indicate that among major tight junction proteins at the blood-brain barrier, *Cldn5* (**C**) and *F11r* (**D**) show an age-dependent downregulation, with correlation coefficients of 0.42 (adjusted P=0.009) and 0.59 (adjusted P=0.0008), respectively. However, no age-dependent downregulation of other tight junction components, such as *Ocln* (**E**) and *Jam3* (**F**), was observed (adjusted P>0.1). Expression values on y axis are reported as transcripts per million.

facilitator superfamily domain-containing 2a protein critical for the formation and maintenance of the BBB.[36] In summary, we find a specific set of genes controlling cerebral EC function being downregulated with increasing age. Next, we asked if such changes are reflected in the epigenetic landscape.

DNA Methylation in Aging cECs

To identify DNA-methylation changes, we performed RRBS on DNA extracted from cECs. Using a 1000-bp window tiling strategy (Methyl-Kit), we identified regions with a minimum of 3 CpGs and showing sufficient coverage across samples. Next, we applied a linear regression analysis (with coverage and sex as covariate) to identify regions associated with age-dependent differentially methylated regions. Overall, we observe only minor changes up to 12 months, followed by a trend of stronger methylation differences at 18 months. (Figure 5A and Figure S12). Most age-dependent Differentially Methylated Regions (710/1000) showed an increase in methylation (hypermethylation and mean change of 9.8%), whereas 210 of 1000 showed a decreased methylation (hypomethylation with a mean change of 69.9%; Figure 5C). A clustering of age-associated single CpGs confirmed this age-dependent trend for single CpGs (Figure 5B). False discovery rate correction reduced the number of significant age-dependent Differentially Methylated Regions to only 12 fulfilling all criteria (Table S7). Remarkably 10 of these 12 regions showed age-dependent hypomethylation, whereas only 2 showed hypermethylation (ie, going against the general trend). Annotation of these top age-dependent Differentially Methylated Regions (Figure 5D) to genes revealed a vicinity to *Gpr56*, *Arid5b*, *Camta1*, *Degs2*, *Sema7a*, and *Zbtb20* (ie, all genes previously shown to be involved in brain [dys] function). *Gpr56 is* a gene coding for a G-protein–coupled receptor previously linked to brain development[37] and multiple sclerosis.[38] For *Arid5b*, methylation dysregulation was reported in a large epigenetic screen for patients with epilepsy[39] and Alzheimer disease.[40] The latter also holds for *Camta1*,[41] which is also linked to age-related macular degeneration[42] and Purkinje cell degeneration[43]; *Degs2* is implicated in schizophrenia[44]; and *Sema7a* was shown to be associated with multiple sclerosis[45,46] and brain development.[47] Finally, *Zbtb20* is associated with the process of neurodevelopment,[48–50] as well as implicated in major depression disorder.[51] Among the 12 genes showing age-dependent methylation dynamics, only 1 gene, *Zbtb20*, was found to be significantly downregulated with age. Together, these findings show that in ECs, one finds epigenetic scars (gain and loss) of methylation in genes linked to brain dysfunctions. Besides *Zbtb*20, however, none of the genes showed a concomitant change in gene expression in ECs.

Chromatin Accessibility in cECs Changes With Age

In total, we identified 33 254 differential open chromatin sites (ATAC peaks) across the samples. A principal component analysis reveals a minor contribution (principal component 3) separating older (12 and 18 months) from younger mice (2 and 6 months). Principal component 2 (5% of the variance) accounts for the differences between males and females. Principal component 1 cannot be explained by age or any other factors, such as sample quality (Figure 6A).

We extracted ATAC enriched open chromatin regions (Table S8) that showed significant change in chromatin accessibility (q-value <0.05). A heat map showed the ATAC signal (normalized per row) across these regions (n=11 694) (Figure 6B), which were annotated afterward with the closest genes (n=4056). As for our analysis of RNA-seq and RRBS data, we used a linear model to account for the effects of sex in the ATAC data. Next, to study the correlation between the age-dependent changes in chromatin accessibility and gene expression, we overlapped the list of differentially accessible genes (n=4056) obtained from ATAC-seq analysis with the list of differentially

Figure 5. Reduced representation bisulfite sequencing (RRBS) of aging cerebral endothelial cells (ECs) to study age-associated changes in methylation.

A, ECs isolated from the brains of 18-month-old mice show increased methylation level compared with the 2-, 6-, and 12-month-old mice. The average methylation level across all the CpGs investigated by RRBS was 70.52% (SD, 0.46%) in the 2-month-old mice, 70.66% (SD, 0.27%) in the 6-month-old mice, 70.46% (SD, 0.53%) in the 12-month-old mice, and 72.30% (SD, 1.17%) in the 18-month-old mice. The average methylation level of CpGs in the ECs isolated from 18-month-old mice is significantly higher in comparison to the 2-, 6-, and 12-month-old mice (adjusted $P<0.01$). However, no significant change in the level of methylation is observed in the 6- or 12-month-old mice in comparison to the 2-month-old mice. Error bars represent mean±SEM. One-way ANOVA, followed by the Tukey honest significant difference test, was performed to compare all the possible pairs. ***$P<0.001$. **B**, Heat map clustering based on top 1000 CpGs associated with aging in the linear regression model does not suggest significant changes in the overall methylation profiles across different samples. **C**, Absolute methylation differences for 2- vs 6-, 12-, and 18-month-old cohorts. To enhance visualization, color gradients were capped at –20% and 20%. The maximum change in the methylation levels is observed between the 2- and 18-month-old groups. **D**–**F**, Methylation dynamics across age groups for the top 3 ranking tiles from the linear regression analysis. The top 3 ranking tiles with the most significant differential methylation dynamics with age were associated with *Gpr56* (**D**), *Arid5b* (**E**), and *Asrgl1* (**F**) genes. To avoid overplotting, data points were subjected to a slight jitter on the *x* axis. Tile location, related gene locus, and obtained *P* value from the linear model are indicated in the respective header. n.s. indicates nonsignificant.

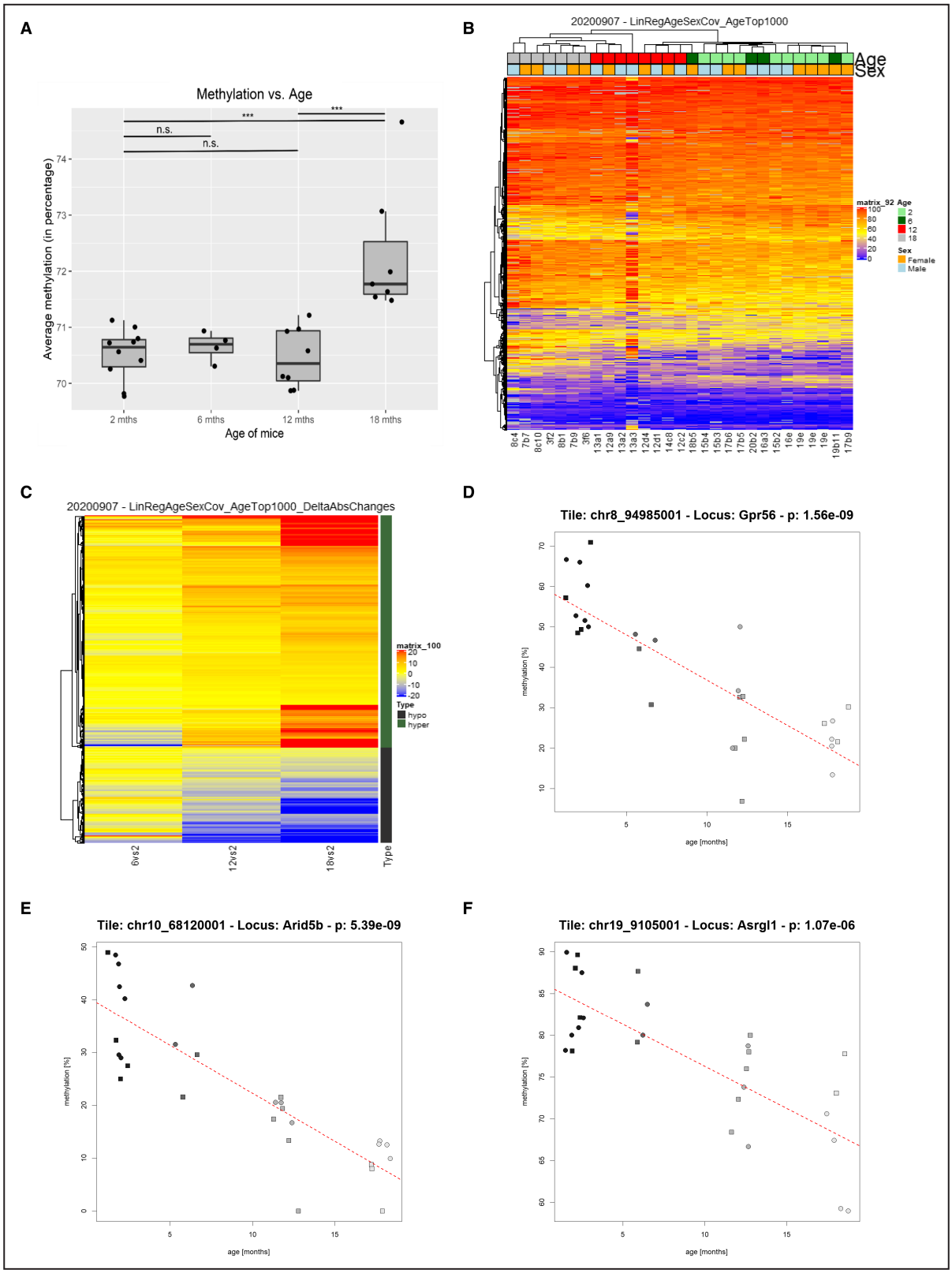

expressed genes (n=1388) extracted from the RNA-seq analysis. We identified 236 genes shared in the 2 gene lists (Figure 6C), including the *Aplnr* gene (Table S9). Interestingly, we also found genes of the Apelin signaling pathway (Kyoto Encyclopedia of Genes and Genomes: mmu04371), such as *Notch3*, *Gnb4*, *Mylk*, and *Akt3*, to show upregulation linked to increased chromatin accessibility. Unlike several

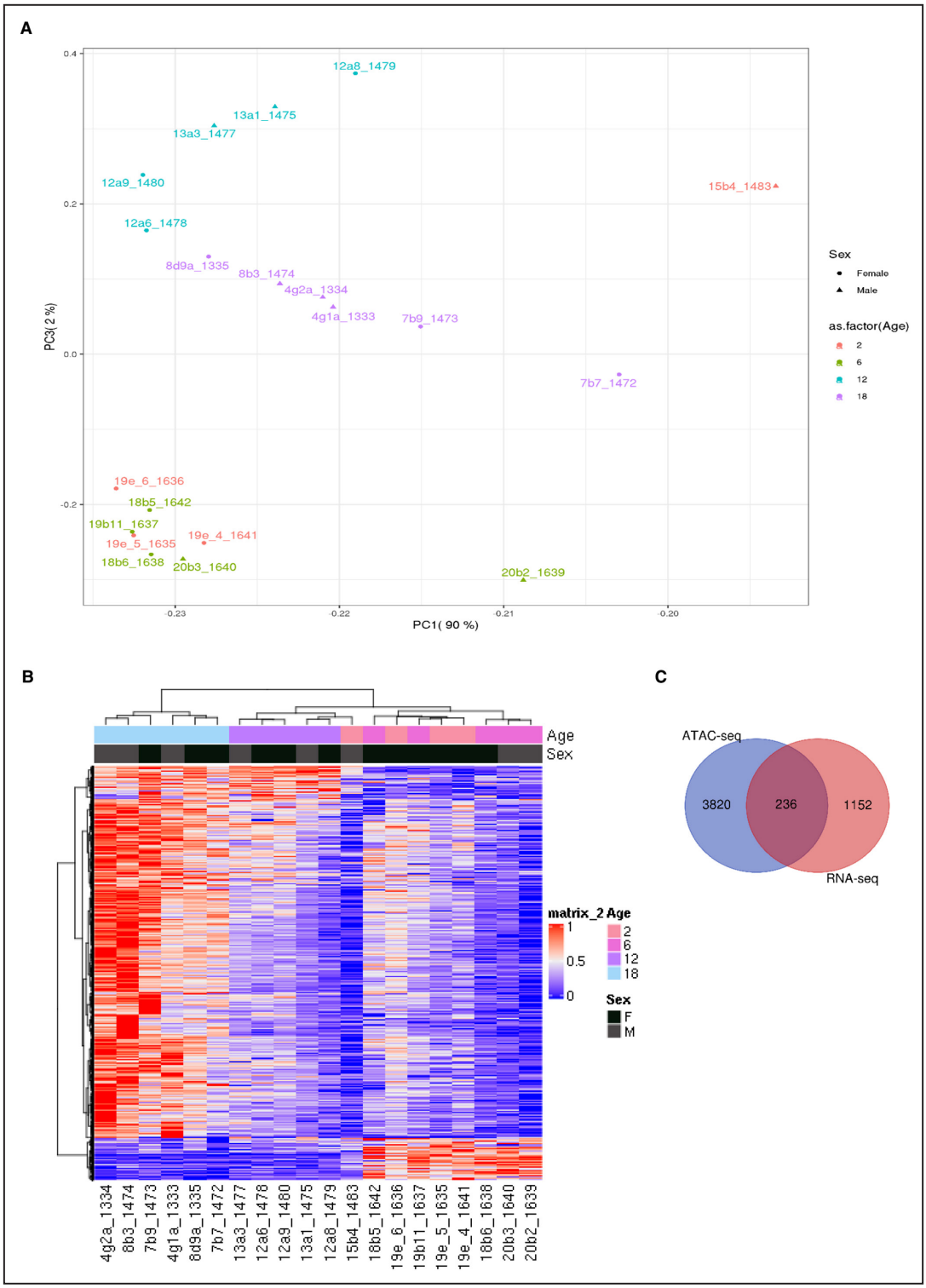

Figure 6. Assay for transposase-accessible chromatin sequencing (ATAC-seq) to study differential chromatin accessibility in aging cerebral endothelial cells.

A, Principal component (PC) analysis of samples (ATAC-seq study). The samples cluster into 2 main groups along PC3: older mice (12 and 18 months) and younger mice (2 and 6 months). PC2 accounts for the differences between the sexes, but the PC1 cannot be explained by any factor. **B**, Heat map showing ATAC signal (normalized per row) in the significant differentially accessible regions (n=11 694). The *x* axis label refers to the sample numbers (mice). The relevant color-coded legends on top indicate age and sex of each sample. **C**, There are 236 genes that overlap between the list of differentially accessible genes (n=4056) obtained from ATAC-seq analysis and the list of differentially expressed genes (n=1388) based on the RNA-sequencing (RNA-seq) analysis.

significant age-associated changes in chromatin accessibility in the vicinity of genes with altered gene expression, such as *Aplnr* and the downstream genes, we do not observe an overlap of DNA-methylation changes with ATAC-enriched regions.

DISCUSSION

In human patients, the genetic basis of several cerebrovascular diseases that affect the integrity of the vasculature in the brain, leading to hemorrhages, has been established in recent years. These include the *CCM1*,*2*,*3* and *KRIT1* genes in cavernous cerebral malformations; *SOX17*, *CNNM2*, *KL/STARD13*, *RBBP8*, and *EDNRA* genes in intracranial aneurysms; *APP*, *BRI2*, *CST3*, *TTR*, and *GSN* genes in cerebral amyloid angiopathy; and *COL4A1* and *COL4A2* genes in COL4-related small-vessel disease. In addition, *HTRA1* and *NOTCH3* genes have been implicated in human cerebral autosomal recessive arteriopathy with subcortical infarcts and leukoencephalopathy and cerebral autosomal dominant arteriopathy with subcortical infarcts and leukoencephalopathy, respectively.[52]

We observed that the incidence of spontaneous cerebral bleeding progressively increases with aging in mice, reflecting the BBB disruption and changes in cerebral vasculature in elderly human patients. Because ECs form the core component of the BBB in the central nervous system vasculature, age-associated changes in vasculature structure and disruption of BBB integrity are likely caused by molecular defects in EC junction structures. Several studies in mice have demonstrated the breakdown of BBB with age, leading to increased BBB permeability.[53,54] In this work, we profiled the age-dependent changes in transcriptomics, genome-wide DNA methylation, and chromatin accessibility in isolated cECs of mice of increasing age. We observed 1388 genes significantly dysregulated with age in the cECs, with 675 genes downregulated and 713 genes upregulated. Among the major tight junction components, *Cldn5* was downregulated with age in the cECs of mice. Claudin-5 is an endothelial-specific, highly expressed, vital component of the tight junctions in the cECs. Interestingly, the *Cldn5* gene is known to be downregulated with age in the cECs of mice, and aged mice exhibit an increased BBB permeability.[54] Other studies have demonstrated the disruption of BBB and impaired vascular integrity with loss of claudin-5.[55,56] Furthermore, we observe age-dependent downregulation of *Itm2a*, a highly expressed endothelial-specific transcript, whose role and function in human or murine ECs has not been well characterized. Cdh2, an adherens junction component, was downregulated with age. Transgenic mice with EC-specific deletion of *Cdh2* display impaired vasculature and are embryonic lethal, suggesting a critical role of N-cadherin in vascular morphogenesis.[57]

Cdc42, a small Rho GTPase, is crucial for maintaining the cytoskeletal dynamics of cells by positively regulating actin polymerization and filopodia formation, which further regulates several cellular processes, such as cell-cell adhesion, cell division, and cell migration. The role of endothelial Cdc42 in EC-EC adhesion is well studied, with endothelial-specific Cdc42 depletion (Cdc42^{Tie2KO} mice) resulting in compromised vasculature, hemorrhages, cerebral vascular malformations,[58] and embryonic lethality.[59] Cdc42 regulates the adhesion between ECs mediated by actin cytoskeletons, which physically support the junction complexes, thereby compromising the vascular integrity.[59] In our RNA-seq data, we observe a significant age-associated downregulation of *Cdc42* and several downstream actors involved in the actin reorganization pathway, such as *Cdc42se1*, *Arf1*, and *Arf6*. The downregulation of *Cdc42* in the aging endothelium might lead to age-associated disruption of the junctional structure at the EC-EC junction, leading to the age-associated breakdown of the BBB and thereby contributing toward increased incidents of cerebral bleedings with age. The actin cytoskeletal dynamics mediated by Cdc42 also regulate Srf, a transcription factor that influences several cellular processes. Interestingly, EC-specific deletion of *Srf* and *Mrtf*, encoding the transcription factors SRF and MRTF-A/B, at either postnatal or adult ages, induces lethal cerebral hemorrhages in mice.[15] We did, however, not observe age-dependent significant dysregulation of *Srf* or *Mrtf* (Figure S13 and Table S10) and note that unaltered mRNA levels do not necessarily exclude altered protein expression or protein activity levels. However, the observed age-associated downregulation of Cdc42 in ECs may alter SRF activity, another possible pathway that might affect the adhesion between ECs and lead to a compromised BBB with age. Any direct roles of endothelial Cdc42 and linked changes in actin dynamics and SRF-regulated target genes remain a possibility, contributing to age-associated BBB disruption, and therefore warrant further investigation.

This study identifies an age-dependent downregulation of the *Htra1* gene, known to regulate TGF-β signaling, which is necessary to maintain vascular integrity. However, the mechanism of *Htra1* regulating the TGF-β signaling pathway is not well established. Although some studies have suggested that Htra1 suppresses TGF-β signaling pathway,[60,61] others have claimed *Htra1* activates the TGF-β signaling pathway.[62] The detailed molecular pathways underlying the role of HTRA1 in development of cerebral autosomal recessive arteriopathy with subcortical infarcts and leukoencephalopathy in human patients are unknown, but HTRA1-mediated dysregulation of TGF-β

signaling pathway could lead to vascular impairment in the central nervous system. However, the detailed mechanisms that link HTRA1 and TGF-β in cECs, and the impact of *Htra1* downregulation on the BBB maintenance, need to be investigated.

We further characterized the changes in DNA methylation with aging in the cECs. Previous studies have reported a reduction in global methylation levels, whereas specific regions may show age-dependent hypermethylation or hypomethylation.[63] In our data, we observed only a mild global overall DNA-methylation change in the cECs on aging, with a slight increase in 18-month-old mice. Evidence from recent age-associated methylation studies in the central nervous system of mice suggests that global methylation levels remain largely stable with age in the hippocampus.[64] The genome-wide methylation levels in the human brain have also been reported to be stable with age[65] but change at particular genes/regions. In our study, we observed significant age-associated methylation changes for 12 regions in the vicinity of genes, such as Gpr56, *Arid5b*, *Camta1*, *Degs2*, *Sema7a*, and *Zbtb20*, previously linked to aging, neurologic development, and diseases. Unlike changes in chromatin accessibility, these DNA methylation changes were not (directly) linked to gene expression changes in the closest gene. In line with previous reports[66]; however, we find age-dependent chromatin accessibility changes that are linked to age-dependent gene expression changes of 236 genes in cECs.

An early and strong age-dependent decrease in chromatin accessibility is found in the promoter region of the *Aplnr* gene. Apelin signaling regulates angiogenic sprouting, endothelial tip cell morphologic characteristics, and sprouting behavior in ECs in zebrafish.[35] Interestingly, fish embryos lacking either the apelin ligand or the apelin receptor have been shown to experience impaired intersegmental vessel formation.[35] Apelin signaling positively regulates EC metabolism, as observed by reduced glycolysis in Apelin signaling–deficient human umbilical vein ECs.[35] In vitro studies have established the role of Apelin receptor in regulating biomechanical and morphologic properties of ECs by regulating signaling pathways that mediate adaptation of ECs to the flow conditions by modulating EC morphologic characteristics, elasticity, adhesion, and spreading.[67] Apelin receptor is known to play a crucial role in positive regulation of vasodilation by heterodimerizing with angiotensin II type 1 receptor, leading to its inhibition, thereby negatively regulating the renin-angiotensin system and promoting vasodilation.[68,69] It has also been reported that Apelin receptor negatively regulates blood pressure in mice. The blood pressure in *Aplnr*$^{-/-}$ mice started to increase at ≈9 months and developed into hypertension when mice attained the age of 12 months.[70] The blood pressure increases with age in both male and female mice, reflecting the pattern observed in humans.[71]

Hypertension is an established major risk factor of intracerebral hemorrhage in humans. *Aplnr* is also known to play a crucial role in positive regulation of vasodilation, and an increased hypertension in mice, rats, and humans has been associated with reduced serum Apelin and disruption of the Apelinergic axis.[72–74] These studies suggest that the age-dependent downregulation of *Aplnr* and its ligand *Apln* in cECs may lead to the activation of the renin-angiotensin system and inhibition of vasodilation, resulting in increased blood pressure in the capillaries. Furthermore, the downregulation of apelinergic axis in mice leads to pathologic signs of accelerated aging, and the infusion of apelin ameliorates age-associated organ impairments and reduces age-associated cardiovascular pathologic conditions in old mice.[70] Our results hint toward a role of the apelin signaling system in age-associated increase in hypertension and increased brain bleeding incidents. In addition, Notch signaling inhibits Apelin signaling. Studies in zebrafish and human umbilical vein EC cell lines established that the downregulation of Notch leads to an increased expression of Apelin. Conversely, the activation of Notch signaling by treating the human umbilical vein ECs with Notch ligand DLL4 leads to the reduction in the levels of Apelin. In our RNA-seq and ATAC-seq data, we observe an age-dependent upregulation of *Notch3*, consistent with the notion that Notch signaling negatively regulates the Apelin signaling pathway.

Our results suggest an involvement of Apelin and its receptor in age-associated changes in cerebral vasculature. Studies have demonstrated the protective role of Apelin in cardiovascular diseases and potential therapeutic targeting of the Apelinergic axis given the highly conserved status of the peptide Apelin among mammals.[75] Although more studies are needed to conclusively establish the mechanisms by which Apelin regulates blood pressure and vasculature, our study further strengthens the avenues of therapeutically targeting the Apelinergic system in the context of cerebrovascular diseases.

ARTICLE INFORMATION

Received May 30, 2023; accepted July 24, 2023.

Affiliations

Interfaculty Institute of Cell Biology, University of Tübingen, Tübingen, Germany (K.M., M.M.O., A.N.); Department of Genetics, University of Saarland, Saarbrücken, Germany (G.G., A.S., J.W.); Genome Analytics, Helmholtz Centre for Infection Research, Braunschweig, Germany (R.G.); Leibniz Institute on Aging, Fritz Lipmann Institute, Jena, Germany (S.H., A.N.); Department of Tissue Morphogenesis, Max Planck Institute for Molecular Biomedicine, Münster, Germany (R.H.A.); Faculty of Medicine, University of Münster, Münster, Germany (R.H.A.); and (K.M., M.M.O., A.N.), International Max Planck Research School "From Molecules to Organisms", Tübingen, Germany.

Acknowledgments

We thank Dr Christine Weinl for her valuable advice on the project, for providing paraformaldehyde-fixed brain samples of mice, and for her advice on histopathology; Dr Kristin Bieber and the staff of the Core Facility Flow Cytometry Berg at the University Hospital Tübingen for help with the fluorescence-activated cell sorting of endothelial cells (ECs); Dr Siegfried Alberti for advice on animal experimentation; and Dr Kishor Kumar Sivaraj for discussion and advice on animal experimentation, as well as the provision of protocols for EC isolation. Author contributions: Kshitij Mohan (KM), Alfred Nordheim (AN), Jörn Walter (JW), and Ralf Adams (RA) designed the study and evaluated the results. KM performed histopathology, microscopic analyses, and data analyses. KM and Michael Orlich (MO) maintained animal colonies, performed animal experiments, and isolated ECs. KM and Gilles Gasparoni (GG) prepared libraries for assay for transposase-accessible chromatin sequencing (ATAC-seq) and reduced representation bisulfite sequencing

(RRBS). GG generated libraries and data of the ATAC-seq study and RRBS. Robert Geffers (RG) was responsible for the RNA-sequencing study. Abdulrahman Salhab (AS), GG, KM, Steve Hoffmann (SH), RG, JW, and AN were responsible for interpretation of data. KM wrote the manuscript. KM, SH, RA, JW, and AN proofread and edited the manuscript.

Sources of Funding

The study was supported by a grant from IMPRS Tübingen "From Molecules to Organisms" to A. Nordheim and Kshitij Mohan. Alfred Nordheim and Michael M. Orlich were funded by the German Research Foundation through SFB/TRR 209–314905040. Gilles Gasparoni was supported by EU H2020 project SYSCID (733100), and Abdulrahman Salhab was supported by the German Federal Ministry of Research and Education grant for de.NBI (031L0101D).

Disclosures

The authors declare no competing interests.

Supplemental Material

Tables S1–S10
Figures S1–S13

REFERENCES

1. GBD 2016 Stroke Collaborators. Global, regional, and national burden of stroke, 1990-2016: a systematic analysis for the Global Burden of Disease Study 2016. *Lancet Neurol*. 2019;18:439–458. doi: 10.1016/S1474-4422(19)30034-1
2. van Asch CJ, Luitse MJ, Rinkel GJ, van der Tweel I, Algra A, Klijn CJ. Incidence, case fatality, and functional outcome of intracerebral haemorrhage over time, according to age, sex, and ethnic origin: a systematic review and meta-analysis. *Lancet Neurol*. 2010;9:167–176. doi: 10.1016/S1474-4422(09)70340-0
3. Jolink WM, Klijn CJ, Brouwers PJ, Kappelle LJ, Vaartjes I. Time trends in incidence, case fatality, and mortality of intracerebral hemorrhage. *Neurology*. 2015;85:1318–1324. doi: 10.1212/WNL.0000000000002015
4. Woo D, Broderick JP. Spontaneous intracerebral hemorrhage: epidemiology and clinical presentation. *Neurosurg Clin N Am*. 2002;13:265–279. doi: 10.1016/S1042-3680(02)00011-6
5. Fisher CM. Pathological observations in hypertensive cerebral hemorrhage. *J Neuropathol Exp Neurol*. 1971;30:536–550. doi: 10.1097/00005072-197107000-00015
6. Harvey A, Montezano AC, Touyz RM. Vascular biology of ageing-implications in hypertension. *J Mol Cell Cardiol*. 2015;83:112–121. doi: 10.1016/j.yjmcc.2015.04.011
7. Obermeier B, Daneman R, Ransohoff RM. Development, maintenance and disruption of the blood-brain barrier. *Nat Med*. 2013;19:1584–1596. doi: 10.1038/nm.3407
8. Abbott NJ, Ronnback L, Hansson E. Astrocyte-endothelial interactions at the blood-brain barrier. *Nat Rev Neurosci*. 2006;7:41–53. doi: 10.1038/nrn1824
9. Montagne A, Zhao Z, Zlokovic BV. Alzheimer's disease: a matter of blood-brain barrier dysfunction? *J Exp Med*. 2017;214:3151–3169. doi: 10.1084/jem.20171406
10. Stamatovic SM, Johnson AM, Keep RF, Andjelkovic AV. Junctional proteins of the blood-brain barrier: new insights into function and dysfunction. *Tissue Barriers*. 2016;4:e1154641. doi: 10.1080/21688370.2016.1154641
11. Olson EN, Nordheim A. Linking actin dynamics and gene transcription to drive cellular motile functions. *Nat Rev Mol Cell Biol*. 2010;11:353–365. doi: 10.1038/nrm2890
12. Weinl C, Riehle H, Park D, Stritt C, Beck S, Huber G, Wolburg H, Olson EN, Seeliger MW, Adams RH, et al. Endothelial SRF/MRTF ablation causes vascular disease phenotypes in murine retinae. *J Clin Invest*. 2013;123:2193–2206. doi: 10.1172/JCI64201
13. Orlich MM, Diéguez-Hurtado R, Muehlfriedel R, Sothilingam V, Wolburg H, Oender CE, Woelffing P, Betsholtz C, Gaengel K, Seeliger M, et al. Mural cell SRF controls pericyte migration, vessel patterning and blood flow. *Circ Res*. 2022;131:308–327. doi: 10.1161/CIRCRESAHA.122.321109
14. Deshpande A, Shetty PMV, Frey N, Rangrez AY. SRF: a seriously responsible factor in cardiac development and disease. *J Biomed Sci*. 2022;29:38. doi: 10.1186/s12929-022-00820-3
15. Weinl C, Castaneda Vega S, Riehle H, Stritt C, Calaminus C, Wolburg H, Mauel S, Breithaupt A, Gruber AD, Wasylyk B, et al. Endothelial depletion of murine SRF/MRTF provokes intracerebral hemorrhagic stroke. *Proc Natl Acad Sci USA*. 2015;112:9914–9919. doi: 10.1073/pnas.1509047112
16. Sindler AL, Delp MD, Reyes R, Wu G, Muller-Delp JM. Effects of ageing and exercise training on eNOS uncoupling in skeletal muscle resistance arterioles. *J Physiol*. 2009;587:3885–3897. doi: 10.1113/jphysiol.2009.172221
17. Bird A. DNA methylation patterns and epigenetic memory. *Genes Dev*. 2002;16:6–21. doi: 10.1101/gad.947102
18. Sivaraj KK, Dharmalingam B, Mohanakrishnan V, Jeong H-W, Kato K, Schröder S, Adams S, Koh GY, Adams RH. YAP1 and TAZ negatively control bone angiogenesis by limiting hypoxia-inducible factor signaling in endothelial cells. *Elife*. 2020;9:e50770. doi: 10.7554/eLife.50770
19. Shih AY, Hyacinth HI, Hartmann DA, van Veluw SJ. Rodent models of cerebral microinfarct and microhemorrhage. *Stroke*. 2018;49:803–810. doi: 10.1161/STROKEAHA.117.016995
20. Reuter B, Venus A, Heiler P, Schad L, Ebert A, Hennerici MG, Grudzenski S, Fatar M. Development of cerebral microbleeds in the APP23-transgenic mouse model of cerebral amyloid angiopathy-a 9.4 Tesla MRI study. *Front Aging Neurosci*. 2016;8:170. doi: 10.3389/fnagi.2016.00170
21. Buenrostro JD, Giresi PG, Zaba LC, Chang HY, Greenleaf WJ. Transposition of native chromatin for fast and sensitive epigenomic profiling of open chromatin, DNA-binding proteins and nucleosome position. *Nat Methods*. 2013;10:1213–1218. doi: 10.1038/nmeth.2688
22. Martin M. Cutadapt removes adapter sequences from high-throughput sequencing reads. *EMBnet. J*. 2011;17:3. doi: 10.14806/ej.17.1.200
23. Dobin A, Davis CA, Schlesinger F, Drenkow J, Zaleski C, Jha S, Batut P, Chaisson M, Gingeras TR. Star: ultrafast universal RNA-seq aligner. *Bioinformatics*. 2013;29:15–21. doi: 10.1093/bioinformatics/bts635
24. Ewels P, Magnusson M, Lundin S, Käller M. MultiQC: summarize analysis results for multiple tools and samples in a single report. *Bioinformatics*. 2016;32:3047–3048. doi: 10.1093/bioinformatics/btw354
25. Love MI, Huber W, Anders S. Moderated estimation of fold change and dispersion for RNA-seq data with DESeq2. *Genome Biol*. 2014;15:550. doi: 10.1186/s13059-014-0550-8
26. Marco-Sola S, Sammeth M, Guigo R, Ribeca P. The GEM mapper: fast, accurate and versatile alignment by filtration. *Nat Methods*. 2012;9:1185–1188. doi: 10.1038/nmeth.2221
27. Zhang Y, Liu T, Meyer CA, Eeckhoute J, Johnson DS, Bernstein BE, Nusbaum C, Myers RM, Brown M, Li W, et al. Model-based analysis of CHiP-Seq (MACS). *Genome Biol*. 2008;9:R137. doi: 10.1186/gb-2008-9-9-r137
28. Li H, Durbin R. Fast and accurate short read alignment with Burrows-Wheeler transform. *Bioinformatics*. 2009;25:1754–1760. doi: 10.1093/bioinformatics/btp324
29. Hovestadt V, Jones DT, Picelli S, Wang W, Kool M, Northcott PA, Sultan M, Stachurski K, Ryzhova M, Warnatz HJ, et al. Decoding the regulatory landscape of medulloblastoma using DNA methylation sequencing. *Nature*. 2014;510:537–541. doi: 10.1038/nature13268
30. Li H, Handsaker B, Wysoker A, Fennell T, Ruan J, Homer N, Marth G, Abecasis G, Durbin R. The Sequence Alignment/Map format and SAMtools. *Bioinformatics*. 2009;25:2078–2079. doi: 10.1093/bioinformatics/btp352
31. Liu Y, Siegmund KD, Laird PW, Berman BP. Bis-SNP: combined DNA methylation and SNP calling for Bisulfite-seq data. *Genome Biol*. 2012;13:R61. doi: 10.1186/gb-2012-13-7-r61

32. Akalin A, Kormaksson M, Li S, Garrett-Bakelman FE, Figueroa ME, Melnick A, Mason CE. Methylkit: a comprehensive R package for the analysis of genome-wide DNA methylation profiles. *Genome Biol*. 2012;13:R87. doi: 10.1186/gb-2012-13-10-r87
33. Liu S, Grigoryan MM, Vasilevko V, Sumbria RK, Paganini-Hill A, Cribbs DH, Fisher MJ. Comparative analysis of H&E and Prussian blue staining in a mouse model of cerebral microbleeds. *J Histochem Cytochem*. 2014;62:767–773. doi: 10.1369/0022155414546692
34. Vanlandewijck M, He L, Mäe MA, Andrae J, Ando K, Del Gaudio F, Nahar K, Lebouvier T, Laviña B, Gouveia L, et al. A molecular atlas of cell types and zonation in the brain vasculature. *Nature*. 2018;554:475–480. doi: 10.1038/nature25739
35. Helker CS, Eberlein J, Wilhelm K, Sugino T, Malchow J, Schuermann A, Baumeister S, Kwon HB, Maischein HM, Potente M, et al. Apelin signaling drives vascular endothelial cells toward a pro-angiogenic state. *Elife*. 2020;9:9. doi: 10.7554/eLife.55589
36. Ben-Zvi A, Lacoste B, Kur E, Andreone BJ, Mayshar Y, Yan H, Gu C. Mfsd2a is critical for the formation and function of the blood-brain barrier. *Nature*. 2014;509:507–511. doi: 10.1038/nature13324
37. Ganesh RA, Venkataraman K, Sirdeshmukh R. GPR56: an adhesion GPCR involved in brain development, neurological disorders and cancer. *Brain Res*. 2020;1747:147055. doi: 10.1016/j.brainres.2020.147055
38. van der Poel M, Ulas T, Mizee MR, Hsiao CC, Miedema SSM, Adelia N, Schuurman KG, Helder B, Tas SW, Schultze JL, et al. Transcriptional profiling of human microglia reveals grey-white matter heterogeneity and multiple sclerosis-associated changes. *Nat Commun*. 2019;10:1139. doi: 10.1038/s41467-019-08976-7
39. Mohandas N, Loke YJ, Hopkins S, Mackenzie L, Bennett C, Berkovic SF, Vadlamudi L, Craig JM. Evidence for type-specific DNA methylation patterns in epilepsy: a discordant monozygotic twin approach. *Epigenomics*. 2019;11:951–968. doi: 10.2217/epi-2018-0136
40. Smith AR, Smith RG, Pishva E, Hannon E, Roubroeks JAY, Burrage J, Troakes C, Al-Sarraj S, Sloan C, Mill J, et al. Parallel profiling of DNA methylation and hydroxymethylation highlights neuropathology-associated epigenetic variation in Alzheimer's disease. *Clin Epigenetics*. 2019;11:52. doi: 10.1186/s13148-019-0636-y
41. Vardarajan BN, Barral S, Jaworski J, Beecham GW, Blue E, Tosto G, Reyes-Dumeyer D, Medrano M, Lantigua R, Naj A, et al. Whole genome sequencing of Caribbean Hispanic families with late-onset Alzheimer's disease. *Ann Clin Transl Neurol*. 2018;5:406–417. doi: 10.1002/acn3.537
42. Sardell RJ, Bailey JN, Courtenay MD, Whitehead P, Laux RA, Adams LD, Fortun JA, Brantley MA Jr, Kovach JL, Schwartz SG, et al. Whole exome sequencing of extreme age-related macular degeneration phenotypes. *Mol Vis*. 2016;22:1062–1076.
43. Long C, Grueter CE, Song K, Qin S, Qi X, Kong YM, Shelton JM, Richardson JA, Zhang CL, Bassel-Duby R, et al. Ataxia and Purkinje cell degeneration in mice lacking the CAMTA1 transcription factor. *Proc Natl Acad Sci USA*. 2014;111:11521–11526. doi: 10.1073/pnas.1411251111
44. Ohi K, Ursini G, Li M, Shin JH, Ye T, Chen Q, Tao R, Kleinman JE, Hyde TM, Hashimoto R, et al. DEGS2 polymorphism associated with cognition in schizophrenia is associated with gene expression in brain. *Transl Psychiatry*. 2015;5:e550. doi: 10.1038/tp.2015.45
45. Gutiérrez-Franco A, Costa C, Eixarch H, Castillo M, Medina-Rodríguez EM, Bribián A, de Castro F, Montalban X, Espejo C. Differential expression of sema3A and sema7A in a murine model of multiple sclerosis: implications for a therapeutic design. *Clin Immunol*. 2016;163:22–33. doi: 10.1016/j.clim.2015.12.005
46. Gutiérrez-Franco A, Eixarch H, Costa C, Gil V, Castillo M, Calvo-Barreiro L, Montalban X, Del Río JA, Espejo C. Semaphorin 7a as a potential therapeutic target for multiple sclerosis. *Mol Neurobiol*. 2017;54:4820–4831. doi: 10.1007/s12035-016-0154-2
47. Jongbloets BC, Lemstra S, Schellino R, Broekhoven MH, Parkash J, Hellemons AJ, Mao T, Giacobini P, van Praag H, De Marchis S, et al. Stage-specific functions of Semaphorin7a during adult hippocampal neurogenesis rely on distinct receptors. *Nat Commun*. 2017;8:14666. doi: 10.1038/ncomms14666
48. Jones KA, Luo Y, Dukes-Rimsky L, Srivastava DP, Koul-Tewari R, Russell TA, Shapiro LP, Srivastava AK, Penzes P. Neurodevelopmental disorder-associated ZBTB20 gene variants affect dendritic and synaptic structure. *PLoS One*. 2018;13:e0203760. doi: 10.1371/journal.pone.0203760
49. Doeppner TR, Herz J, Bähr M, Tonchev AB, Stoykova A. ZBTB20 regulates developmental neurogenesis in the olfactory bulb and gliogenesis after adult brain injury. *Mol Neurobiol*. 2019;56:567–582. doi: 10.1007/s12035-018-1104-y
50. Nagao M, Ogata T, Sawada Y, Gotoh Y. ZBTB20 promotes astrocytogenesis during neocortical development. *Nat Commun*. 2016;7:11102. doi: 10.1038/ncomms11102
51. Davies MN, Krause L, Bell JT, Gao F, Ward KJ, Wu H, Lu H, Liu Y, Tsai PC, Collier DA, et al. Hypermethylation in the ZBTB20 gene is associated with major depressive disorder. *Genome Biol*. 2014;15:R56. doi: 10.1186/gb-2014-15-4-r56
52. Karschnia P, Nishimura S, Louvi A. Cerebrovascular disorders associated with genetic lesions. *Cell Mol Life Sci*. 2019;76:283–300. doi: 10.1007/s00018-018-2934-5
53. Stamatovic SM, Martinez-Revollar G, Hu A, Choi J, Keep RF, Andjelkovic AV. Decline in Sirtuin-1 expression and activity plays a critical role in blood-brain barrier permeability in aging. *Neurobiol Dis*. 2019;126:105–116. doi: 10.1016/j.nbd.2018.09.006
54. Elahy M, Jackaman C, Mamo JC, Lam V, Dhaliwal SS, Giles C, Nelson D, Takechi R. Blood-brain barrier dysfunction developed during normal aging is associated with inflammation and loss of tight junctions but not with leukocyte recruitment. *Immun Ageing*. 2015;12:2. doi: 10.1186/s12979-015-0029-9
55. Nitta T, Hata M, Gotoh S, Seo Y, Sasaki H, Hashimoto N, Furuse M, Tsukita S. Size-selective loosening of the blood-brain barrier in claudin-5-deficient mice. *J Cell Biol*. 2003;161:653–660. doi: 10.1083/jcb.200302070
56. Greene C, Hanley N, Campbell M. Claudin-5: gatekeeper of neurological function. *Fluids Barriers CNS*. 2019;16:3. doi: 10.1186/s12987-019-0123-z
57. Luo Y, Radice GL. N-cadherin acts upstream of VE-cadherin in controlling vascular morphogenesis. *J Cell Biol*. 2005;169:29–34. doi: 10.1083/jcb.200411127
58. Castro M, Laviña B, Ando K, Álvarez-Aznar A, Taha AA, Brakebusch C, Dejana E, Betsholtz C, Gaengel K. CDC42 deletion elicits cerebral vascular malformations via increased MEKK3-dependent KLF4 expression. *Circ Res*. 2019;124:1240–1252. doi: 10.1161/CIRCRESAHA.118.314300
59. Barry DM, Xu K, Meadows SM, Zheng Y, Norden PR, Davis GE, Cleaver O. Cdc42 is required for cytoskeletal support of endothelial cell adhesion during blood vessel formation in mice. *Development*. 2015;142:3058–3070. doi: 10.1242/dev.125260
60. Graham JR, Chamberland A, Lin Q, Li XJ, Dai D, Zeng W, Ryan MS, Rivera-Bermúdez MA, Flannery CR, Yang Z. Serine protease HTRA1 antagonizes transforming growth factor-β signaling by cleaving its receptors and loss of HTRA1 in vivo enhances bone formation. *PLoS One*. 2013;8:e74094. doi: 10.1371/journal.pone.0074094
61. Shiga A, Nozaki H, Yokoseki A, Nihonmatsu M, Kawata H, Kato T, Koyama A, Arima K, Ikeda M, Katada S, et al. Cerebral small-vessel disease protein HTRA1 controls the amount of TGF-beta1 via cleavage of proTGF-beta1. *Hum Mol Genet*. 2011;20:1800–1810. doi: 10.1093/hmg/ddr063
62. Beaufort N, Scharrer E, Kremmer E, Lux V, Ehrmann M, Huber R, Houlden H, Werring D, Haffner C, Dichgans M. Cerebral small vessel disease-related protease HTRA1 processes latent TGF-beta binding protein 1 and facilitates TGF-beta signaling. *Proc Natl Acad Sci USA*. 2014;111:16496–16501. doi: 10.1073/pnas.1418087111
63. Xiao FH, Kong QP, Perry B, He YH. Progress on the role of DNA methylation in aging and longevity. *Brief Funct Genomics*. 2016;15:454–459. doi: 10.1093/bfgp/elw009
64. Hadad N, Masser DR, Blanco-Berdugo L, Stanford DR, Freeman WM. Early-life DNA methylation profiles are indicative of age-related transcriptome changes. *Epigenetics Chromatin*. 2019;12:58. doi: 10.1186/s13072-019-0306-5
65. Wagner M, Steinbacher J, Kraus TF, Michalakis S, Hackner B, Pfaffeneder T, Perera A, Muller M, Giese A, Kretzschmar HA, et al. Age-dependent levels of 5-methyl-, 5-hydroxymethyl-, and 5-formylcytosine in human and mouse brain tissues. *Angew Chem Int Ed Engl*. 2015;54:12511–12514.
66. Benayoun BA, Pollina EA, Brunet A. Epigenetic regulation of ageing: linking environmental inputs to genomic stability. *Nat Rev Mol Cell Biol*. 2015;16:593–610. doi: 10.1038/nrm4048
67. Strohbach A, Pennewitz M, Glaubitz M, Palankar R, Gross S, Lorenz F, Materzok I, Rong A, Busch MC, Felix SB, et al. The apelin receptor influences biomechanical and morphological properties of endothelial cells. *J Cell Physiol*. 2018;233:6250–6261. doi: 10.1002/jcp.26496
68. Siddiquee K, Hampton J, McAnally D, May L, Smith L. The apelin receptor inhibits the angiotensin II type 1 receptor via

allosteric trans-inhibition. *Br J Pharmacol*. 2013;168:1104–1117. doi: 10.1111/j.1476-5381.2012.02192.x
69. Wu D, He L, Chen L. Apelin/APJ system: a promising therapy target for hypertension. *Mol Biol Rep*. 2014;41:6691–6703. doi: 10.1007/s11033-014-3552-4
70. Rai R, Ghosh AK, Eren M, Mackie AR, Levine DC, Kim SY, Cedernaes J, Ramirez V, Procissi D, Smith LH, et al. Downregulation of the apelinergic axis accelerates aging, whereas its systemic restoration improves the mammalian healthspan. *Cell Rep*. 2017;21:1471–1480. doi: 10.1016/j.celrep.2017.10.057
71. Barsha G, Denton KM, Mirabito Colafella KM. Sex- and age-related differences in arterial pressure and albuminuria in mice. *Biol Sex Differ*. 2016;7:57. doi: 10.1186/s13293-016-0110-x
72. Goetze JP, Rehfeld JF, Carlsen J, Videbaek R, Andersen CB, Boesgaard S, Friis-Hansen L. Apelin: a new plasma marker of cardiopulmonary disease. *Regul Pept*. 2006;133:134–138. doi: 10.1016/j.regpep.2005.09.032
73. Chandra SM, Razavi H, Kim J, Agrawal R, Kundu RK, de Jesus PV, Zamanian RT, Quertermous T, Chun HJ. Disruption of the apelin-APJ system worsens hypoxia-induced pulmonary hypertension. *Arterioscler Thromb Vasc Biol*. 2011;31:814–820. doi: 10.1161/ATVBAHA.110.219980
74. Alastalo TP, Li M, Perez Vde J, Pham D, Sawada H, Wang JK, Koskenvuo M, Wang L, Freeman BA, Chang HY, et al. Disruption of PPARγ/β-catenin-mediated regulation of apelin impairs BMP-induced mouse and human pulmonary arterial EC survival. *J Clin Invest*. 2011;121:3735–3746. doi: 10.1172/JCI43382
75. Zhong J-C, Zhang Z-Z, Wang W, McKinnie SMK, Vederas JC, Oudit GY. Targeting the apelin pathway as a novel therapeutic approach for cardiovascular diseases. *Biochim Biophys Acta Mol Basis Dis*. 2017;1863:1942–1950. doi: 10.1016/j.bbadis.2016.11.007